

Gramaccioliite-(Y): paragenesis chemistry, and structure in a new occurrence, Samos Island, Greece

THOMAS THEYE^{1,*}, FRÉDÉRIC HATERT², EWALD OCKENGA³, CHRISTIAN BERTOLDI⁴ and CHRISTIAN LATHE⁵

¹ Institute for Mineralogy und Crystal Chemistry, University of Stuttgart, Azenbergstr. 18, D-70174 Stuttgart, Germany

*Corresponding author, e-mail: thomas.theye@imi.uni-stuttgart.de

² Laboratory of Mineralogy, B-18, University of Liège, B-4000 Liège, Belgium

³ Steintorwall 8, D-38100 Braunschweig, Germany

⁴ Division for Mineralogy, University of Salzburg, Hellbrunnerstraße 34, A-5020 Salzburg, Austria

⁵ Helmholtz-Zentrum Potsdam, Deutsches GeoForschungsZentrum GFZ, Sektion 5.1, Telegrafenberg, D-14473 Potsdam, Germany

Abstract: We describe a second occurrence of the recently defined mineral species gramaccioliite-(Y), a member of the crichtonite group, on Samos Island, Greece. The mineral occurs in form of centimetre-sized crystals in brecciated metabauxite, associated with diaspore, hematite, muscovite, chloritoid, calcite, rutile, monazite-(Ce), and REE carbonate minerals (bastnäsite-(La) and parisite-(Ce)). Petrological observations indicate that the coarse-grained vein assemblage containing gramaccioliite-(Y), diaspore and chloritoid was succeeded by calcite, rutile, monazite-(Ce) and hematite/limonite, suggesting a chronological relation such as: gramaccioliite-(Y) + fluid \rightarrow monazite + rutile + hematite. Latest stage alteration is characterized by the formation of fine-grained kaolinite + calcite + limonite. The petrographical observations suggest that gramaccioliite-(Y), because of the contemporaneous formation with chloritoid and diaspore, was formed at a temperature of about 400 °C, *i.e.* under metamorphic conditions.

A high-pressure experiment was conducted to examine the *P-T* stability of gramaccioliite-(Y). Neither phase transformations nor formations of other phases were observed up to 50 kbar, 1100 °C under dry conditions, indicating that this mineral may be stable down the Earth's mantle.

An electron-microprobe examination reveals that gramaccioliite-(Y) from Samos Island contains a significant amount of REE, and has accordingly a distinct miscibility towards davidite-(La). In contrast, gramaccioliite-(Y) from the type locality contains a relatively high amount of crichtonite (s.s.) component. A characteristic feature of the examined Samos material is growth zoning within single crystals, mainly concerning Pb being enriched and REE being depleted in the cores.

A single-crystal structure refinement of gramaccioliite-(Y) was performed to $R_1 = 0.0308$ in space group $R\bar{3}$, with $a = 9.1814(5)$ Å and $\alpha = 68.820(4)^\circ$, $Z = 1$. The crystal structure is topologically identical to those of minerals of the crichtonite group, with M0 occupied by Pb and La, M1 occupied by Y, Sc, Ce, Zr, Dy and Mn^{2+} , M2 occupied by Fe^{2+} and Zn, M3 occupied by Fe^{3+} , Ti and Al, M4 and M5 occupied by Ti.

Key-words: gramaccioliite-(Y), davidite-(La), crichtonite group, Samos, Greece, rare earth elements, stability.

1. Introduction

Gramaccioliite-(Y), ideally $PbY(Ti,Fe)_{20}O_{38}$, is a member of the crichtonite group which comprises a complex series of oxide minerals with the general formula $AM_{21}O_{38}$ (Grey *et al.* 1976). To account for different structural sites, Orlandi *et al.* (1997) re-wrote the formula as $X^{II}A^{VI}B^{VI}C^{IV}_{18}T_2O_{38}$ (notation used in this paper: A = M0, B = M1, T = M2, C = M3/M4/M5). The members of this group so far defined are cleusonite, crichtonite, davidite-(La), davidite-(Y), davidite-(Ce), dessauite-(Y), gramaccioliite-(Y), landauite, lindsayite, loveringite, mathiasite, and senaite (Table 1; *cf.* Wülsler *et al.*, 2005).

Most of these minerals have been discovered only in the last 30 years. Gramaccioliite-(Y) belongs to the most recently defined ones, discovered in a hydrothermal deposit in the Argentera Massif, Italy (Orlandi *et al.*, 2004). Hitherto, only this occurrence was known, as well as a sample of unknown origin described by the same authors. We found a new location of this rare mineral in metamorphic rocks from Samos Island, Greece. Because the chemical composition of the Samos gramaccioliite-(Y) significantly deviates from those described by Orlandi *et al.* (2004), we present comprehensive data on chemical composition, petrological significance, and crystal structure, as well as a preliminary examination of the *P-T* stability until 1100 °C, 50 kbar.

Table 1. Main cations on the M0 (=A) and M1 (=B) structural sites of the crichtonite group minerals. REE = rare earth elements.

	M0 site	M1 site
cleusonite	Pb	U
crichtonite	Sr	Mn
davidite-(Y)	REE	Y
davidite-(La)	REE	REE
davidite-(Ce)	REE	REE
dessauite-(Y)	Sr	Y
gramaccioliite-(Y)	Pb	Y
landauite	Na	Mn
lindsleyite	Ba	Zr
loveringite	Ca	Zr
mathiasite	K	Zr
Senaite	Pb	Mn

2. Occurrence and geological setting

The new occurrence of gramaccioliite-(Y) was discovered on the eastern coast of Samos Island (Greece) in a location called Mikri Lakka, where a ~ 130 m sized body of low-grade metamorphic bauxite occurs embedded in calcite marble. Samples studied in this paper were taken in the vicinity of an abandoned quarry in which the metabauxite has been mined as raw material for abrasive and aluminium production. The metamorphic overprint of the metabauxite-bearing Vourliotes Unit occurred under high-pressure conditions (M1, metamorphosed about 55 Ma ago, P-T conditions estimated to ~ 450 °C, 10–15 kbar) followed by a greenschist-facies overprint (M2, 20–25 Ma ago) (Chen & Okrusch, 1992; Will *et al.*, 1998; Ring & Layer, 2003).

The metabauxite body, in general, is only slightly affected by metamorphic deformation and shows a well preserved pisolithic microstructure. Major minerals of this rock are diaspore and hematite. Muscovite and chloritoid may also be present in this rock, as well as the minor minerals tourmaline, spinel and zincohögbonite (Ockenga, 2000). Due to a pre-metamorphic enrichment of elements such as Ni, Co, and Zn at the footwall of the metabauxite lens (*cf.*, Maksimović & De Weisse, 1979; Feenstra & Maksimović, 1985; Ockenga, 2000), a more variegated mineralogy is present in this position. Actually, a metabauxite in western Samos is the type locality of zincohögbonite (Ockenga *et al.*, 1998). Moreover, Li-rich zincostaurolite (Feenstra *et al.*, 2003) and Co-rich gahnite (Feenstra, 1997; Ockenga, 2000) have been described from the footwall of the eastern Samos metabauxite.

In addition to the presence of unusual mineral compositions, the footwall boundary between the metabauxite and the marble is affected by intensive and multiphase brecciation and hydrothermal veining. The vein mineralogy comprises calcite, diaspore, and muscovite as the major minerals. Hematite, rutile, chloritoid, REE carbonate minerals (bastnäsite, parisite), monazite and gramaccioliite-(Y) are locally present. The grain size of these minerals may reach more than 1 cm.

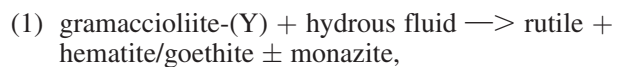
3. Paragenesis and petrological significance

In the studied samples, gramaccioliite-(Y) occurs in brecciated veins which are characterized by the presence of angular fragments of metabauxite and of marble with interstitial space filled by relatively coarse-grained vein precipitates. In a final stage of metamorphic history, fine-grained intergrowths of calcite, kaolinite, and limonite occur, partly replacing the previously formed minerals.

Main vein minerals comprise centimetre-sized muscovite, diaspore, and chloritoid. All these minerals are in apparent chemical equilibrium. The diaspore + chloritoid assemblage suggests a formation at low-grade metamorphic conditions, in the range of 400 °C, being compatible with the previous estimations (Chen & Okrusch, 1992; Will *et al.*, 1998). Relatively coarse-grained diaspore is also enclosed in gramaccioliite-(Y), attesting that this mineral represents not an early, low-temperature but metamorphic formation (Fig. 1a). In a later stage of vein history, the large crystals are partly cataastically fragmented, with cracks filled by calcite (Fig. 1a, b). Likewise, rutile crystallized lately; it mainly appears at the rims of gramaccioliite-(Y) (Fig. 1b). As further REE mineral, relatively small-sized monazite occurs either in the lately formed matrix composed of limonite, calcite and kaolinite (Fig. 1c), or associated to (altered) matrix being present in large gramaccioliite-(Y) crystals (Fig. 1d). Apparently, monazite formed along with late-stage alteration minerals in the fine-grained matrix.

Coarse-grained REE carbonate minerals present in the altered matrix comprise intergrown bastnäsite and parisite. No clear structural relations have been observed between REE carbonates and gramaccioliite-(Y), but similar grain sizes suggest a roughly contemporaneous growth, *i.e.* under metamorphic conditions. The same holds true for the formation of partly centimetre-sized chloritoid and muscovite.

According to the petrographical observations, rutile as well as monazite has apparently been formed later than gramaccioliite-(Y). An allochemical reaction relating these minerals could have been:



with a hydrous fluid removed Pb, Y and HREE and delivered LREE and P. Reaction (1) could represent mainly a temporal sequence with variations in the composition of the fluid phase being the driving force. Alternatively, variation of metamorphic *P* and *T* could be considered. Investigations of Janots *et al.* (2006) on low-*T* metamorphic rocks show that allanite and REE carbonate are present at high *P* (12–16 kbar), whereas at lower *P* of 3–10 kbar monazite and florencite occur instead. In line with these results, in Samos a paragenesis of REE carbonates and gramaccioliite-(Y) could have grown at high *P* during the M1 metamorphic episode, and monazite later at lower *P* during M2.

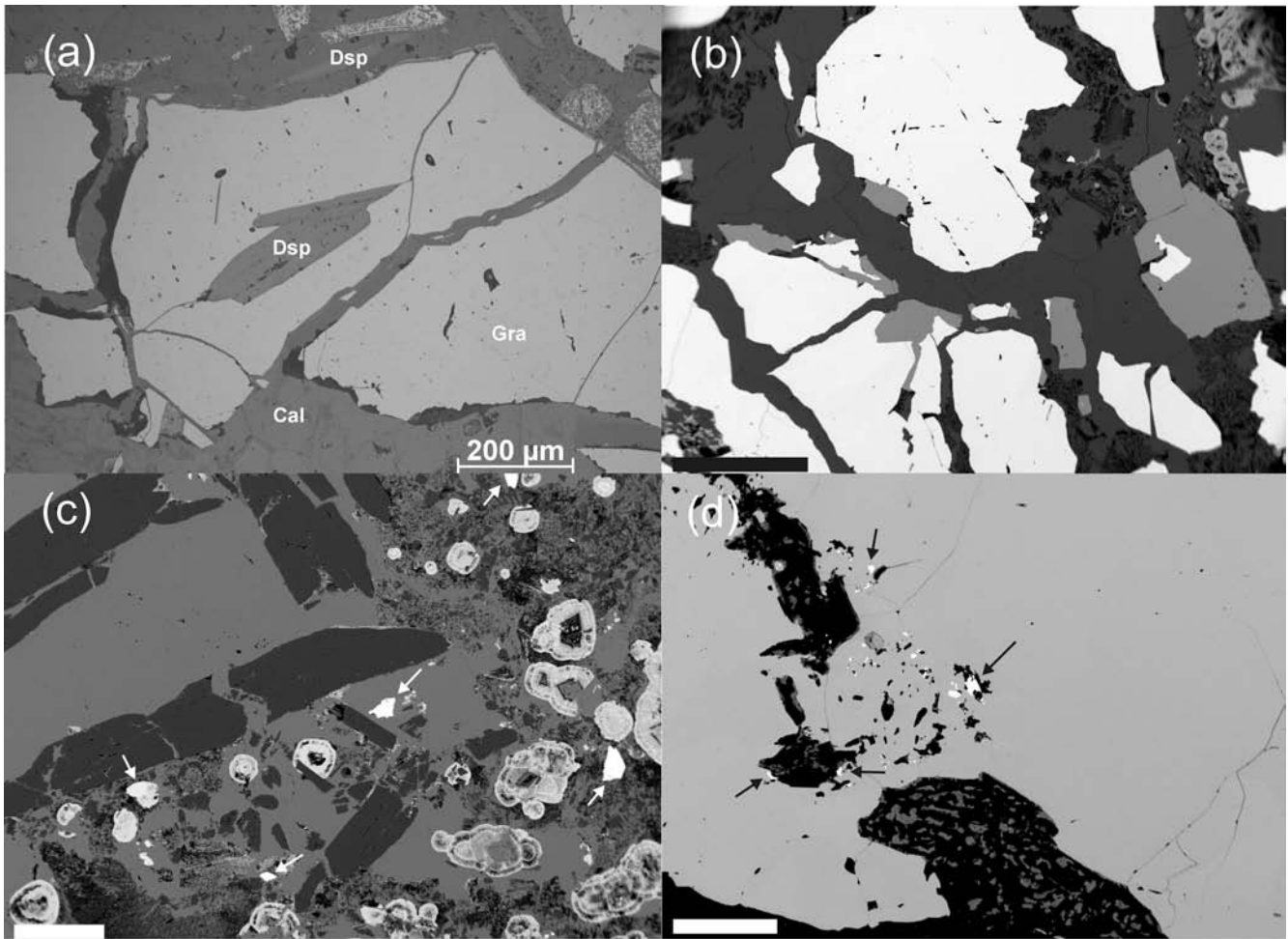


Fig. 1. Gramaccioliite-(Y) bearing veins in metabauxite, Samos Island, Greece. (a) Brecciated gramaccioliite-(Y) with inclusions of euhedral diaspore and cracks filled by calcite. Note that gramaccioliite-(Y) fragments perfectly fit together. The matrix is composed of calcite. Reflected light image. (b) Gramaccioliite-(Y) (white grains) partly rimmed by rutile (light grey). The matrix mainly consists of calcite (dark) and limonite (upper right). Back scattered electron (BSE) image. Scale bar is 500 μm . (c) Small monazite-(Ce) (white grains, arrows) in a matrix of calcite (intermediate grey). Limonite (bright grey) shows concentric growth structures. Dark crystals with euhedral columnar outlines are diaspore. The heterogeneous, fine-grained portion of the matrix is a mixture of kaolinite, calcite and limonite. BSE image. Scale bar is 200 μm . (d) Monazite-(Ce) (bright phase, arrows) inclusions in a large grain of gramaccioliite-(Y) are always associated with the late-stage phases kaolinite, limonite, and calcite (dark/black). BSE image. Scale bar is 200 μm .

4. Chemical composition of gramaccioliite-(Y) and coexisting minerals

A CAMECA SX100 electron microprobe equipped with five WD spectrometers was used for the microchemical analyses on polished thin sections. The operation conditions were 15 kV, 10–60 nA, focussed beam (defocussed for carbonate analyses). The standards used were diopside (Mg, Ca), corundum (Al), Cr_2O_3 (Cr), Fe_2O_3 (Fe), TiO_2 (Ti), rhodonite (Mn), sphalerite (Zn), Sc (Sc), Zr (Zr), PbTe (Pb), synthetic phosphates (REE, P) and synthetic U (U) and ThO_2 (Th). The counting times were between 20 and 210 s both on peak and on background positions. The raw data have been processed with the PAP software (Pouchou & Pichoir, 1984) delivered by CAMECA. For a typical gramaccioliite-(Y) composition, the 1σ uncertainty as calculated on the base of counting statistics is

<0.2 wt% for Ti, Fe, Pb, and <0.03 wt% for other measured elements.

Ferrous iron was measured with an oxidimetric method on a purified mineral sample, separated by handpicking and subsequent removal of calcite with diluted HCl. The results of two measurements of the bulk sample are 6.67 and 6.76 wt% FeO. Because the total iron content analysed by the microprobe is fairly constant (Table 2a), we assume that the FeO content of gramaccioliite-(Y) is also roughly constant in the whole sample. Accordingly, the FeO content analysed on the bulk mineral sample is considered to be the same for all microprobe analyses. Fe_2O_3 is calculated by subtracting FeO from the total iron measured with the microprobe. Water and CO_2 have quantitatively been analysed with IR spectroscopy on the separated mineral. The results are 0.15 and 0.20 wt%, respectively. These low contents are considered as not belonging to the

Table 2a. Chemical analyses of gramaccioliite-(Y), formulae normalized to 38 oxygen. bdl = below detection limit; FeO as due to wet-chemical analysis.

SerNo.	grain 1 4	grain 1 7	grain 1 10	grain 1 11	grain 2 1	grain 2 4	grain 2 6	grain 2 7	grain 3 2	grain 3 3	grain 3 10	grain 3 11
TiO ₂	52.28	52.34	52.81	52.54	52.93	53.09	53.19	53.23	53.14	52.80	53.01	52.89
Cr ₂ O ₃	0.14	0.16	0.12	0.07	0.12	0.15	0.19	0.15	0.07	0.16	0.12	0.17
Al ₂ O ₃	0.77	0.82	0.77	0.78	0.80	0.86	0.77	0.86	0.80	0.80	0.87	0.88
Fe ₂ O ₃	20.78	20.71	20.22	20.27	20.48	19.99	19.90	20.04	19.79	19.91	20.13	20.11
FeO	6.72	6.72	6.72	6.72	6.72	6.72	6.72	6.72	6.72	6.72	6.72	6.72
MnO	0.21	0.20	0.20	0.21	0.20	0.22	0.21	0.23	0.21	0.22	0.22	0.22
ZnO	0.75	0.69	0.58	0.59	0.64	0.65	0.69	0.66	0.64	0.68	0.69	0.69
ZrO ₂	0.47	0.56	0.64	0.65	0.53	0.84	0.64	0.78	0.56	0.55	0.58	0.59
Sc ₂ O ₃	0.53	0.51	0.38	0.38	0.40	0.61	0.53	0.67	0.63	0.63	0.64	0.64
CaO	0.04	0.04	0.04	0.04	0.05	0.07	0.05	0.04	0.04	0.04	0.03	0.03
Y ₂ O ₃	3.28	3.23	3.18	3.15	3.25	2.65	2.91	2.65	2.98	3.01	2.96	2.97
La ₂ O ₃	3.63	3.37	2.07	2.13	2.70	1.78	1.49	1.80	2.07	2.02	2.72	2.64
Ce ₂ O ₃	1.35	1.25	19.9	0.79	1.00	0.72	0.51	0.64	0.78	0.73	1.05	0.99
Pr ₂ O ₃	0.07	0.08	bdl	bdl	bdl	0.03	0.03	0.04	0.05	0.05	0.03	0.00
Nd ₂ O ₃	0.09	0.09	0.06	0.10	0.06	0.07	0.04	0.05	0.09	bdl	0.06	0.08
Sm ₂ O ₃	0.06	0.07	0.09	0.08	0.09	0.05	0.09	0.05	bdl	0.08	0.05	0.02
Gd ₂ O ₃	0.40	0.40	0.37	0.44	0.43	0.32	0.41	0.32	0.36	0.39	0.36	0.36
Dy ₂ O ₃	0.63	0.55	0.56	0.55	0.59	0.48	0.58	0.47	0.60	0.60	0.54	0.55
Er ₂ O ₃	0.50	0.50	0.45	0.43	0.44	0.39	0.49	0.48	0.49	0.45	0.51	0.48
Yb ₂ O ₃	0.34	0.37	0.29	0.33	0.31	0.35	0.36	0.35	0.34	0.33	0.34	0.38
La ₂ O ₃	3.63	3.37	2.07	2.13	2.70	1.78	1.49	1.80	2.07	2.02	2.72	2.64
Ce ₂ O ₃	1.35	1.25	0.82	0.79	1.00	0.72	0.51	0.64	0.78	0.73	1.05	0.99
PbO	4.73	5.23	7.67	7.70	6.59	8.19	8.93	8.44	7.89	7.88	6.74	6.72
ThO ₂	0.08	0.11	0.23	0.21	0.16	0.26	0.24	0.17	0.20	0.18	0.20	0.21
UO ₂	bdl	bdl	bdl	bdl	bdl	0.06	0.03	0.03	bdl	bdl	bdl	bdl
Σ	97.85	98.03	98.24	98.17	98.47	98.51	98.97	98.87	98.47	98.15	98.57	98.35
Ti	12.572	12.581	12.759	12.722	12.708	12.778	12.816	12.781	12.810	12.766	12.717	12.707
Cr	0.036	0.041	0.030	0.018	0.031	0.038	0.048	0.037	0.018	0.040	0.030	0.044
Al	0.290	0.310	0.290	0.297	0.301	0.326	0.291	0.322	0.300	0.301	0.329	0.330
Fe ³⁺	4.998	4.979	4.886	4.909	4.919	4.812	4.795	4.812	4.772	4.816	4.829	4.833
Fe ²⁺	1.796	1.796	1.805	1.809	1.793	1.798	1.800	1.794	1.801	1.806	1.792	1.795
Zn	0.176	0.164	0.138	0.141	0.139	0.151	0.154	0.162	0.156	0.152	0.160	0.162
Σ	19.868	19.871	19.908	19.896	19.891	19.903	19.904	19.908	19.857	19.881	19.857	19.871
Sc	0.147	0.143	0.106	0.108	0.112	0.171	0.149	0.187	0.176	0.177	0.177	0.178
Mn	0.056	0.054	0.054	0.057	0.054	0.061	0.056	0.061	0.057	0.059	0.059	0.061
Y	0.557	0.550	0.543	0.539	0.551	0.452	0.497	0.451	0.509	0.514	0.503	0.505
Zr	0.073	0.087	0.100	0.102	0.082	0.131	0.100	0.122	0.088	0.086	0.091	0.092
Nd	0.011	0.010	0.007	0.011	0.007	0.008	0.005	0.006	0.010	0.004	0.006	0.009
Sm	0.007	0.008	0.010	0.009	0.010	0.005	0.010	0.005	0.002	0.008	0.005	0.002
Gd	0.042	0.043	0.040	0.047	0.046	0.034	0.044	0.034	0.038	0.041	0.038	0.039
Dy	0.065	0.056	0.058	0.058	0.061	0.049	0.060	0.048	0.062	0.062	0.055	0.056
Er	0.051	0.050	0.045	0.043	0.045	0.039	0.050	0.048	0.050	0.046	0.051	0.048
Yb	0.033	0.036	0.029	0.033	0.030	0.034	0.035	0.034	0.033	0.032	0.033	0.037
Pb	0.407	0.450	0.663	0.667	0.566	0.706	0.770	0.725	0.681	0.682	0.579	0.578
Th	0.006	0.008	0.017	0.016	0.012	0.019	0.017	0.012	0.014	0.013	0.015	0.015
U	0.000	0.000	0.000	0.000	0.000	0.004	0.002	0.002	0.000	0.000	0.000	0.000
La	0.429	0.398	0.245	0.253	0.318	0.210	0.176	0.212	0.245	0.239	0.320	0.311
Ce	0.158	0.147	0.096	0.093	0.117	0.085	0.060	0.074	0.092	0.085	0.123	0.116
Pr	0.008	0.010	0.001	0.003	0.002	0.002	0.004	0.004	0.005	0.005	0.003	0.000
ΣA	2.050	2.050	2.014	2.039	2.013	2.010	2.035	2.025	2.062	2.053	2.058	2.047

gramaccioliite-(Y) but being due to inclusions of calcite, diaspore or muscovite.

It can be observed in the back-scattered electron images that single grains of gramaccioliite-(Y) are chemically heterogeneous (Fig. 2). The zoning appears, in many cases, as an oscillatory growth zoning (Fig. 2, grain 1)

being consistent with a hydrothermal formation of this mineral. Pb-rich, REE-poor compositions often appear in the cores (bright in BSE images), whereas darker rims are characterized by REE-rich compositions. Other grains show an unsystematic variation (Fig. 2, grain 2) which seems to have been formed by amalgamation and

Table 2b. Analyses of monazite (Mona, formulae normalized to 3 oxygen), bastnäsite (Bast, 1 cation) and of parisite (Par, 3 cations).

	Par	Par	Bast	Bast	Bast	Mona	Mona	Mona
SiO ₂						0.21	0.19	0.15
P ₂ O ₅						29.22	28.94	29.13
SO ₃						0.05	0.03	0.02
CaO	10.36	11.15	0.38	0.63	0.51	0.36	0.36	0.21
Y ₂ O ₃	1.75	1.60	0.55	0.57	0.60	0.40	0.31	0.46
La ₂ O ₃	17.42	16.96	27.45	26.89	26.45	20.88	21.28	21.06
Ce ₂ O ₃	19.32	18.59	24.12	24.40	24.51	21.54	22.02	22.13
Pr ₂ O ₃	3.18	3.55	3.54	3.54	3.45	3.84	3.65	3.45
Nd ₂ O ₃	13.97	13.93	12.85	13.39	13.66	15.75	15.39	15.36
Sm ₂ O ₃	2.46	2.41	1.72	1.81	1.66	2.75	2.63	2.76
Gd ₂ O ₃	2.24	2.16	1.35	1.36	1.33	2.10	1.96	2.30
Dy ₂ O ₃	0.68	0.80	0.35	0.32	0.31	0.37	0.29	0.46
ThO ₂	1.15	1.39	2.20	1.54	1.56	1.56	1.38	1.16
F	5.62	5.39	7.85	8.06	8.20			
H ₂ O ^a	0.71	0.89	0.36	0.30	0.20			
CO ₂ ^a	24.71	25.23	19.94	20.12	19.95			
O=F	-2.37	-2.27	-3.31	-3.40	-3.45			
Σ	101.19	101.78	99.37	99.54	98.93	99.01	98.43	98.65
Ca	0.987	1.049	0.015	0.025	0.020	0.015	0.015	0.009
Y	0.083	0.074	0.011	0.011	0.012	0.008	0.007	0.010
La	0.571	0.547	0.373	0.362	0.359	0.307	0.316	0.311
Ce	0.629	0.597	0.325	0.325	0.329	0.314	0.324	0.324
Pr	0.103	0.113	0.047	0.047	0.046	0.056	0.054	0.050
Nd	0.444	0.435	0.169	0.174	0.179	0.224	0.221	0.220
Sm	0.075	0.072	0.022	0.023	0.021	0.038	0.036	0.038
Gd	0.066	0.062	0.017	0.016	0.016	0.028	0.026	0.031
Dy	0.019	0.022	0.004	0.004	0.004	0.005	0.004	0.006
Th	0.023	0.028	0.018	0.013	0.013	0.014	0.013	0.011
Σ	3.000	3.000	1.000	1.000	1.000	1.009	1.015	1.009
F	1.579	1.484	0.912	0.928	0.952			
H	0.421	0.516	0.088	0.072	0.048			
C	3.000	3.000	1.000	1.000	1.000			
Si						0.008	0.008	0.006
P						0.986	0.985	0.987
S						0.002	0.001	0.001
Σ						0.996	0.993	0.994

^astoichiometry.

cementation of fragmented pieces, in addition to growth zoning. Grain 3 (Fig. 2) is fairly homogeneous. This grain has been used for crystal structure refinement.

About 50 microprobe analyses have been carried out of gramaccioliite-(Y). Its chemical composition is governed by TiO₂ and Fe-oxide accompanied by smaller amounts of Al, Ca, Cr, Mn, Pb, REE, Sc, Th, Y, Zn, and Zr. Other elements are present only in subordinate amounts, below detection limit of the electron microprobe at the selected analysis conditions. This particularly holds true for uranium that is an important component of most published davidite analyses. The most important components besides Ti and Fe are PbO with 7.1 ± 1.2 (1σ) wt%, and Y₂O₃ with 3.0 ± 0.2 wt%. As can be seen from Fig. 2, Y is fairly constant in all analyses, but Pb shows a more important variation.

In Table 2, the mineral formulae are calculated on the basis of 38 oxygen, and considering the wet-chemically

analysed Fe²⁺ content of the bulk sample. The average cation total is 21.93 atoms per formula unit (*apfu*), indicating that there is only small deficiency with respect to the ideal value of 22. The Italian gramaccioliite-(Y), in contrast, has a much higher deficiency (21.36 *apfu*; Orlando *et al.*, 2004). A formal grouping of the various cations according to ion size results in an average value of 19.88 for the relatively small sized cations Ti, Al, Fe, Cr, and Zn which can be assessed to the M2 to M5 positions of the gramaccioliite-(Y) structure. The remaining larger-sized M0 and M1 cations Ca, Sc, Mn, La, Ce Pr, Nd, Sm, Gd, Dy, Er, Yb, Y, Pb, Th, U, and Zr result in an average total of about 2.04 *apfu*. Although partitioning of similar sized and charged cations between M0 and M1 positions can be expected, it can be expected from the analyses that Y is always the predominant cation on the intermediate-sized M1 site, and Pb on the larger M0 site. This assignment is confirmed by the single-crystal X-ray diffraction study

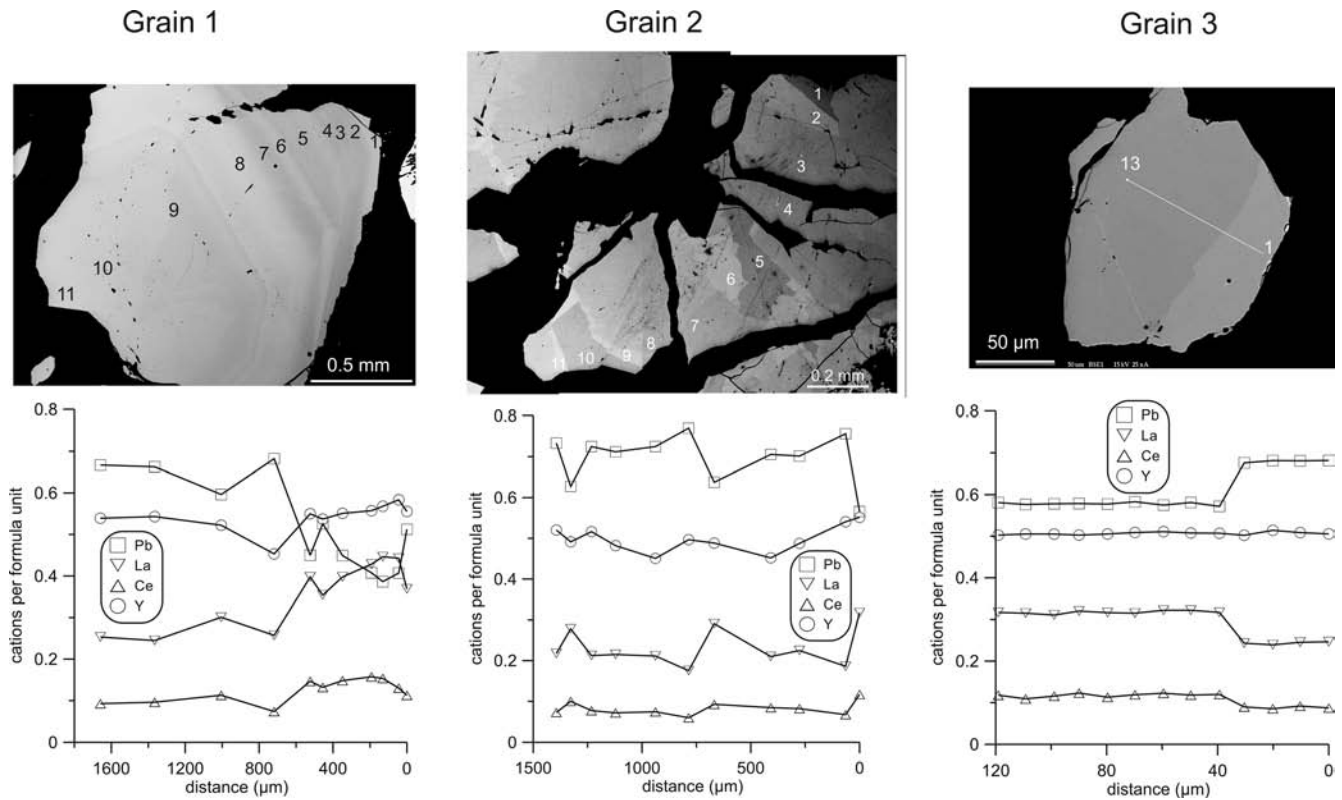


Fig. 2. Back scattered electron images and compositional profiles of gramacciolite-(Y) grains. (a) Grain 1 shows a concentric compositional zoning with a Pb-rich core and a REE-rich/Pb-poor rim of davidite-(La) composition. (b) In grain 2, an irregular zoning is present. (c) Grain 3 was used for the crystal structure refinement and shows a minor heterogeneity only.

(see below). The majority of the analysed spots can therefore be classified as gramacciolite-(Y) as defined by Orlandi *et al.* (2004). Only a few analyses (rim of grain 1 in Fig. 2) have less Pb and a higher content of LREE, and are therefore classified as davidite-(La).

A chemical line profile in grain 1 (Fig. 2) shows a systematic variation from core to rim. The core is characterized by higher Pb content with up to 0.7 *apfu*, whereas the rim contains a higher amount of REE (except the very rim of grain 1). The content of Y is relatively constant throughout all grains at about 0.5 *apfu*.

Compared to the original material studied by Orlandi *et al.* (2004), the sample from Samos shows some significant variations in the cationic distributions. The large M0 site of the original material contains significant Sr, whereas in the Samos sample LREE elements are present in larger amounts besides Pb (Table 2a). In the intermediate-sized M1 site, HREE, Sc, and Zr are also present in a significant amount besides Y, in contrast to the Orlandi *et al.* (2004) samples, where it is Mn. Accordingly, the original material has a miscibility towards crichtonite, $\text{SrMn}(\text{Ti},\text{Fe})_{20}\text{O}_{38}$, whereas the Samos sample reveals a mixing towards davidite-(La), $(\text{La},\text{Ce},\text{U})_2(\text{Ti},\text{Fe})_{20}\text{O}_{38}$.

The chemical compositions of bastnäsite and parsite are dominated by light REE with La and Ce, respectively, being the most prominent one. These minerals are therefore classified as bastnäsite-(La) and parsite-(Ce). The fluorine content is lower than the ideal one, suggesting

the presence of OH. In monazite, Ce is the most abundant REE. Accordingly, it is classified as monazite-(Ce). The chemical compositions of chloritoid (with $\text{Fe}^{2+}/(\text{Fe}^{2+}+\text{Mg}) = 0.95$) and muscovite are homogeneous and close to end-member. Selected analyses of monazite-(Ce), bastnäsite-(La) and parsite-(Ce) are given in Table 2b.

5. REE distribution pattern

For the examination of the distribution of REE of gramacciolite-(Y), the contents are normalised to a chondrite average (Schmitt *et al.*, 1964; Fig. 3). It can be seen that gramacciolite-(Y) is characterized by a U-shaped distribution pattern. The LREE La and Ce as well as the HREE Gd to Yb are relatively enriched, whereas the intermediate sized ones Pr, Nd, and Sm are depleted. This behaviour of gramacciolite-(Y) is reflecting the existence of two different structural positions, the M0 site hosting LREE (mainly La and Ce) and the M1 site more suitable for HREE+Y (mainly Gd, Dy, Er, Yb, Y), respectively. It is also concluded that this mineral may act as an important carrier of both very light and very heavy REE, as well as of yttrium. In contrast, monazite, bastnäsite, and parsite display a very strong enrichment of LREE, and a depletion of HREE+Y, as reported from elsewhere (e.g., Janots *et al.*, 2006).

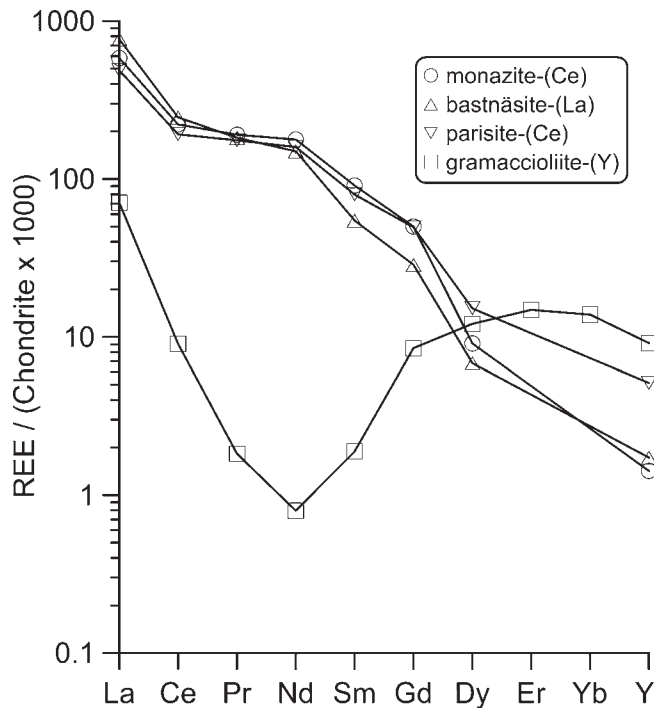


Fig. 3. Chondrite-normalized REE-patterns of monazite-(Ce), bastnäsite-(La), parisite-(Ce), and gramaccioliite-(Y). Chondrite REE abundances by Schmitt *et al.* (1964).

6. X-ray diffraction study

The X-ray powder diffraction pattern of gramaccioliite-(Y) from Samos Island was recorded with a Bruker-AXS D8 Advance powder X-ray diffractometer, equipped with a Cu tube and secondary graphite monochromator. The peak positions were calibrated against silicon that was used as internal standard. The following unit-cell parameters fitted to a hexagonal cell were refined (23 reflections): $a = 10.375(1)$ Å, $c = 20.872(4)$ Å, $V = 1945.6(4)$ Å³. These values are very close to those of $a = 10.382$ Å, $c = 20.882$ Å obtained from single-crystal data by Orlandi *et al.* (2004).

From the separated concentrate of gramaccioliite-(Y), a suitable isometric grain of 150 µm in size was selected for the single-crystal X-ray diffraction study. The same crystal as for the structure refinement was measured with the electron microprobe. For this purpose, the grain was embedded in resin and polished. It turned out that the grain is chemically slightly heterogeneous (grain 3 in Fig. 2 and Table 2a). However, compared to grain 1 and 2, the chemical zoning is not significant in grain 3 selected for the X-ray diffraction study.

The X-ray structural study was carried out on an Oxford Diffraction Xcalibur diffractometer (MoK α radiation, $\lambda = 0.71073$ Å) equipped with a Sapphire2 CCD-area detector (Ruhr-Universität Bochum, Germany), on a crystal fragment of $0.10 \times 0.15 \times 0.17$ mm. 645 frames with a spatial resolution of 1° were collected by the ϕ/ω scan technique, with a counting time of 10 s per frame, in the range $5.98^\circ < 2\theta < 86.02^\circ$ ($-15 \leq h \leq 16$, $-16 \leq k \leq 17$, $-16 \leq l \leq 16$). 12177 reflections were extracted from these

frames, corresponding to 2987 unique reflections. The unit-cell parameters refined from these reflections are $a = 9.1814(5)$ Å and $\alpha = 68.820(4)^\circ$ (equivalent to $a = 10.3770$ and $c = 20.8719$ Å in hexagonal notation). Data were corrected for Lorenz polarisation and absorption effects, the latter with a numerical method included in the CrysAlisRED package (Oxford Diffraction, 2002).

The crystal structure was refined in space group $R\bar{3}$, which was confirmed from systematic absences. The starting atomic coordinates were those of gramaccioliite-(Y) from the Massif of Argentera, Italy (Orlandi *et al.*, 2004), and scattering curves for neutral atoms, together with anomalous dispersion corrections, were taken from the *International Tables for X-ray Crystallography, Vol. C* (Wilson, 1992). Cation occupancies were refined to obtain a better agreement with the chemical composition of gramaccioliite-(Y) (Table 2a). For the sake of simplicity, Cr, Sc, Mn, Zn, Zr, Ce, Pr, Nd, Sm, Gd, Er, Yb, Ca, Th, and U, which generally occur in low amounts, were not taken into account in the crystal structure refinement. Finally, the relative occupancies of Pb and La on the M0 site, of Y and Dy on the M1 site, of Fe and vacancies on the M2 and M3 sites, and of Ti and vacancies on the M4 and M5 sites, were refined. The refinement was completed using equivalent displacement parameters for all atoms. The final conventional R_1 factor is 0.0308. Further details on the intensity data collection and structure refinement are given in Table 3. Final positional and equivalent thermal

Table 3. Experimental details for the single-crystal X-ray diffraction study of gramaccioliite-(Y) from Samos Island, Greece.

Dimensions of the crystal (mm)	ca. $0.10 \times 0.15 \times 0.17$
a (Å)	9.1814(5)
α (°)	68.820(4)
Space group	$R\bar{3}$
Z	1
Calculated density	4.776 g/cm ³
Diffractometer	Oxford Diffraction Xcalibur with Sapphire2 CCD-area detector
Operating conditions	50 kV, 30 mA
Radiation	MoK α ($\lambda = 0.71073$ Å)
Scan mode	ϕ/ω scans
$2\theta_{\min}$, $2\theta_{\max}$	5.98°, 86.02°
Range of indices	$-15 \leq h \leq 16$, $-16 \leq k \leq 17$, $-16 \leq l \leq 16$
Measured intensities	12177
Unique reflections	2987
Independent non-zero [$I > 2\sigma(I)$] reflections	1810
Absorption correction	Numerical
μ (mm ⁻¹)	12.73
I.s. refinement program	SHELXL-97 (Sheldrick, 1997)
Refined parameters	99
R_1 [on $I > 2\sigma(I)$]	0.0311
R_1 (all)	0.0664
wR_2 (all)	0.0356
S (goodness of fit)	0.898
Max Δ/σ in the last I.s. cycle	0.025
Max peak and hole in the final ΔF map (e/Å ³)	+1.12 and -1.25

Table 4. Final fractional coordinates (x , y , z) and equivalent displacement parameters (U_{eq}) for gramaccioliite-(Y) from Samos Island, Greece.

Site	x	y	z	U_{eq}
M0	0	0	0	0.0287(1)
M1	0.5	0.5	0.5	0.0082(1)
M2	0.30902(3)	0.30902(3)	0.30902(3)	0.0092(2)
M3	0.34765(4)	0.02013(4)	0.12621(4)	0.00805(9)
M4	0.31027(4)	0.14689(4)	0.72038(4)	0.0086(1)
M5	0.47401(4)	0.64479(4)	0.07911(4)	0.0083(1)
O1	0.3010(2)	0.3772(2)	0.6290(2)	0.0110(3)
O2	0.1492(2)	0.9377(2)	0.2365(2)	0.0118(3)
O3	0.9184(2)	0.3017(2)	0.4589(1)	0.0102(3)
O4	0.1441(2)	0.9894(2)	0.5147(2)	0.0112(3)
O5	0.3884(2)	0.1352(2)	0.4857(2)	0.0099(3)
O6	0.7099(2)	0.0698(2)	0.2419(2)	0.0113(3)
O7	0.2130(1)	0.2130(1)	0.2130(1)	0.0101(5)

parameters are given in Table 4. Anisotropic thermal parameters are given as Supplementary material (Table S1), freely available online on the GSW website of the journal (<http://eurjmin.geoscienceworld.org/>). Selected bond distances are given in Table 5.

The basic features of the gramaccioliite-(Y) structure are identical to those of other minerals of the crichtonite group, and we refer to the previous literature for a detailed description of this structure (Grey *et al.*, 1976; Gatehouse *et al.*, 1979; Orlandi *et al.*, 2004). Due to the good quality of the gramaccioliite-(Y) crystal investigated herein and to the accurate data collection, we were able to refine also the anisotropic displacement parameters for the O atoms, a refinement which was not possible on the crystal originally investigated by Orlandi *et al.* (2004). This feature, together with the detailed refinement of the site occupancies, is responsible for the R_1 value of 0.0308, much lower than the R_1 value 0.0861 obtained by Orlandi *et al.* (2004).

A detailed cationic distribution has also been established, in order to match as closely as possible the average

Table 5. Selected bond distances (\AA) in gramaccioliite-(Y) from Samos Island, Greece.

M0-O2	2.758(2) \times 6	M4-O2	1.866(1)
M0-O6	2.821(1) \times 6	M4-O3	1.937(1)
<u>Average</u>	<u>2.790</u>	M4-O1	1.955(1)
		M4-O6	1.958(1)
M1-O1	2.230(1) \times 6	M4-O5	2.040(1)
		M4-O6'	2.085(1)
M2-O5	1.963(1) \times 3	<u>Average</u>	<u>1.974</u>
M2-O7	2.004(3)	M5-O4	1.839(1)
<u>Average</u>	<u>1.973</u>	M5-O1	1.880(1)
M3-O4	1.951(1)	M5-O3	1.936(1)
M3-O3	1.981(1)	M5-O5	1.982(1)
M3-O2	2.007(1)	M5-O6	2.020(1)
M3-O7	2.007(1)	M5-O5'	2.190(1)
M3-O4'	2.015(1)	<u>Average</u>	<u>1.975</u>
M3-O2'	2.089(1)		
<u>Average</u>	<u>2.008</u>		

chemical composition of gramaccioliite-(Y) reported in Table 2a. The results given in Table 6 indicate that the refined site populations (RSP), obtained from the single-crystal structure refinement, are in good agreement with the assigned site populations (ASP), deduced from the chemical data. Moreover, the refined site scattering values (RSS) and the mean bond lengths (MBL) obtained from the structural data are very close to the calculated site scattering values (CSS) and the calculated bond lengths (CBL), respectively (Table 6). This agreement confirms the reliability of the assigned site populations.

The bond-valence table for gramaccioliite-(Y) is given in Table 7, where the bond-valence sums were calculated as $s = \exp[(R_0 - R)/0.37]$, by using R_0 values of Brown & Altermatt (1985) and Brown (2002) (Ce, La). The bond valences for oxygen are close to the theoretical value 2.00, and a good correspondence is observed between the theoretical and the calculated valence values for the cationic sites (Table 7). For the M0 site, the calculated bond-valence sum (2.04 v.u.) is significantly lower than the valence expected for the cations occurring on this site (2.10 v.u.). This feature is probably related to the lone-electron pairs of the Pb atoms, which need to be located in large structural cavities (Fig. 4) as those occurring in the mineral shannonite, $\text{Pb}_2\text{O}(\text{CO}_3)$ (Krivovichev & Burns, 2000). For cations with lone-electron pairs, as for example Se^{4+} , Bi^{3+} , Sb^{3+} or Pb^{2+} , it has been shown that a modification of the bond-valence concept was required to calculate reliable bond-valence sums (Wang & Liebau, 1996).

7. P-T stability of gramaccioliite-(Y)

Most occurrences of crichtonite group minerals are from low-pressure, low to high-temperature environments such as igneous rocks, pegmatites, and hydrothermal mineralizations, including the type material of gramaccioliite-(Y) itself. Reports of these minerals in metamorphic rocks are rare. Wölser *et al.* (2005) reported cleusonite that occurs in greenschist-facies metamorphic rocks. As suggested above, a metamorphic temperature of about 400 °C can also be expected for the material under current discussion. Crichtonite group minerals (mainly lindsleyite and mathiasite) also rarely occur in mantle derived kimberlites and metasomized peridotites (e.g., Haggerty *et al.*, 1983; Wang *et al.*, 1999), *i.e.*, formed under very high P and T .

An experimental high-pressure/high-temperature study on our natural gramaccioliite-(Y) was carried out with a cubic multi-anvil press of the MAX-80 type (*cf.* Duffy & Wang, 1998), installed at the DORIS III storage ring of HASYLAB (Hamburger Synchrotron Strahlungslabor). The white synchrotron radiation passes through the slits between the gliding anvils of the press. The diffracted radiation was measured with a 2048 channel Canberra EDS detector under a fixed diffraction angle of about 7°20'. Details of the experimental arrangement are similar to that described by Peun *et al.* (1995) and Grevel *et al.* (2000). For the sample, we used high-pressure cells made

Table 6. Refined site populations (RSP, $apfu$), refined site-scattering values (RSS, $epfu$), mean bond lengths (MBL, Å), assigned site populations (ASP, $apfu$), calculated site-scattering values (CSS, $epfu$), and calculated bond lengths (CBL, Å) for gramaccioliite-(Y) from Samos Island, Greece. The ASP derived from the chemical analysis is simplified, neglecting minor cations.

Site	Results of the structure determination			Results of the chemical analysis			CSS	CBL ^a
	RSP	RSS	MBL	ASP	CSS			
M0	0.486 Pb + 0.514 La	69.3	2.790	0.600 Pb + 0.300 La			66.3	2.867
M1	0.895 Y + 0.105 Dy	42.0	2.230	0.530 Y + 0.200 Sc + 0.100 Ce + 0.070 Zr + 0.050 Dy + 0.050 Mn ²⁺			38.0	2.324
M2	0.966 Fe	25.1	1.973	0.900 Fe ²⁺ + 0.100 Zn			26.4	2.047
M3	0.905 Fe	23.5	2.008	0.820 Fe ³⁺ + 0.120 Ti + 0.060 Al			24.7	2.054
M4	0.976 Ti	21.5	1.974	1.000 Ti			22.0	2.025
M5	0.976 Ti	21.5	1.975	1.000 Ti			22.0	2.025

^a The CBL values have been calculated from the ASP, by using the effective ionic radii of Shannon (1976).

Table 7. Bond-valence table (vu) for gramaccioliite-(Y) from Samos Island, Greece.

	M0	M1	M2	M3	M4	M5		Σ
O1	0.000	0.510*	0.000	0.000	0.685	0.841		2.036
O2	0.184*	0.000	0.000	0.512	0.870	0.000	1.566	1.977
O2'	0.000	0.000	0.000	0.411	0.000	0.000	0.411	
O3	0.000	0.000	0.000	0.548	0.719	0.721		1.989
O4	0.000	0.000	0.000	0.595	0.000	0.937	1.532	2.034
O4'	0.000	0.000	0.000	0.502	0.000	0.000	0.502	
O5	0.000	0.000	0.532**	0.000	0.545	0.638	1.715	2.078
O5'	0.000	0.000	0.000	0.000	0.000	0.363	0.363	
O6	0.155*	0.000	0.000	0.000	0.680	0.577	1.412	1.894
O6'	0.000	0.000	0.000	0.000	0.482	0.000	0.482	
O7	0.000	0.000	0.477	0.513	0.000	0.000		2.016
$S_{\text{calc.}}$	2.04	3.06	2.07	3.08	3.98	4.08		
$S_{\text{theor.}}$	2.10	3.02	2.00	3.12	4.00	4.00		

The bond valences were calculated from the bond lengths given in Table 5, and from the assigned site populations of Table 6, with the parameters of Brown & Altermatt (1985) and Brown (2002) (Ce, La). Bond valences were multiplied by 6 (*) or by 3 (**), for the calculation of the valence on the M0, M1 and M2 crystallographic sites.

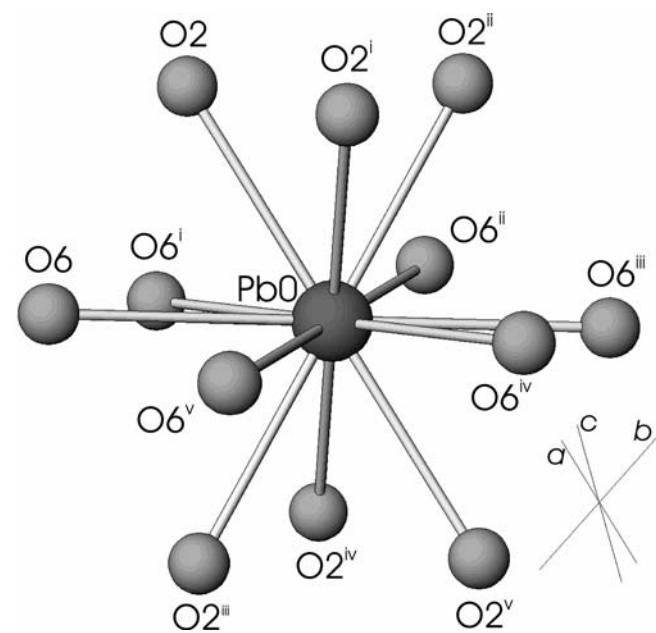


Fig. 4. Coordination polyhedron of the M0 site in gramaccioliite-(Y) from Samos.

of boron with 8 mm in edge length. In order to ensure the hydrostatic behaviour of the samples under high-pressure conditions, the samples were mixed with NaCl. The pressure was calibrated using the NaCl equation of state (Decker, 1971). The temperature was measured with a thermocouple directly placed into the sample volume. The overall uncertainty is considered to be 3 kbar for pressure, and 30 °C for temperature.

During the first 3 hours of the experiment, at first P and then T were increased up to 50 kbar and 1100 °C. Then, the experiment was held for additional 30 min at the maximal conditions. During this time, neither breakdown of gramaccioliite-(Y) nor growth of an additional phase was observed, suggesting that this mineral was stable at these conditions. It can be concluded that gramaccioliite-(Y) has a very large P - T stability ranging from hydrothermal (Orlandi *et al.*, 2004) to mantle conditions.

Acknowledgements: We would like to thank Heinz-Jürgen Bernhardt and Thomas Fockenberg, both Ruhr-Universität Bochum, for providing us a mineral formula calculation software, and for performing the ferrous iron analysis,

respectively. F.H. acknowledges H. Graetsch for his help during the X-ray measurements at the Ruhr-Universität Bochum, Germany, as well as the FRS-F.N.R.S. (Belgium) for a position of "Chercheur Qualifié". Useful and constructive advice of two anonymous referees and of the journal editors C. Chopin, M. Pasero and E. Tillmanns is also gratefully acknowledged.

References

Brown, I.D. (2002): The chemical bond in inorganic chemistry. The bond valence model. Oxford University Press, Oxford, 278 p.

Brown, I.D. & Altermatt, D. (1985): Bond-valence parameters obtained from a systematic analysis of the inorganic crystal structure database. *Acta Cryst.*, **B41**, 244–247.

Chen, G. & Okrusch, M. (1992): The high pressure blueschist facies metamorphism on Samos, Greece: a study of metapelites by the Schreinemakers-method. *Ber. Dtsch. Mineral. Ges., Beih. z. Eur. J. Mineral.*, **4**, 1, 53.

Decker, D.L. (1971): High-pressure equation of state for NaCl, KCl, and CsCl. *J. Appl. Phys.*, **42**, 3239–3244.

Duffy, T.S. & Wang, Y. (1998): Pressure-volume-temperature equations of state. *Rev. Mineral.*, **37**, 425–457.

Feeenstra, A. (1997): Zincohögbomite and gahnite in a diaspore-bearing metabauxite from eastern Samos (Greece): mineral chemistry, element partitioning and reaction relations. *Schweiz. Mineral. Petrogr. Mitt.*, **77**, 73–93.

Feeenstra, A. & Maksimović, Z. (1985): Geochemistry of diaspore and corundum-bearing metabauxites from Naxos, Greece. Part II: The existence of premetamorphic trace element patterns in amphibolite facies metabauxite lenses and their use as geochemical top and bottom indicators. in "Metamorphism of Bauxites on Naxos, Greece", A. Feeenstra. *Geologica Ultraiectina*, **39**, 175–206.

Feeenstra, A., Ockenga, E., Rhede, D., Wiedenbeck, M. (2003): Li-rich zincostaurolite and its decompression related breakdown products in a diaspore-bearing metabauxite from East Samos (Greece): An EMP and SIMS study. *Am. Mineral.*, **88**, 789–805.

Gatehouse, B.M., Grey, I.E., Kelly, P.R. (1979): The crystal structure of davidite. *Am. Mineral.*, **64**, 1010–1017.

Grevel, K.-D., Nowlan, E.U., Fasshauer, D.W., Burchard, M. (2000): In situ X-ray investigation of lawsonite and zoisite at high pressures and temperatures. *Am. Mineral.*, **85**, 206–216.

Grey, I.E., Lloyd, D.J., White, J.S. Jr. (1976): The structure of crichtonite and its relationship to senaite. *Am. Mineral.*, **61**, 1203–1212.

Haggerty, S.E., Smyth, J.R., Erlank, A.J., Rickard, R.S., Danchin, R.V. (1983): Lindsleyite (Ba) and Mathiasite (K): two new chromium-titanates in the crichtonite series from the upper mantle. *Am. Mineral.*, **68**, 494–505.

Janots, E., Negro, F., Brunet, F., Goffé, B., Engi, M., Bouybaouène, M.L. (2006): Evolution of REE mineralogy in HP-LT metapelites of the Sebtide complex, Rif, Morocco: Monazite stability and geochronology. *Lithos*, **87**, 214–234.

Krivovichev, S.V. & Burns, P.C. (2000): Crystal chemistry of basic lead carbonates. I. Crystal structure of synthetic shannonite, $Pb_2O(CO_3)_2$. *Mineral. Mag.*, **64**, 1063–1068.

Maksimović, Z. & De Weisse, G. (1979): Geochemical study in an overturned bauxite deposit in Les Codouls (S. France). *Travaux ICSOBA*, **15**, 109–120.

Ockenga, E. (2000): Petrologie und Geochemie von Metabauxiten der Zentral- und Ost-Ägäis (Griechenland). Dissertation, Würzburg, 221 p.

Ockenga, E., Yalçın, Ü., Medenbach, O., Schreyer, W. (1998): Zincohögbomite, a new mineral from eastern Aegean metabauxites. *Eur. J. Mineral.*, **10**, 1361–1366.

Orlandi, P., Pasero, M., Duchi, G., Olmi, F. (1997): Dessauite, $(Sr,Pb)(Y,U)(Ti,Fe^{3+})_{20}O_{38}$, a new mineral of the crichtonite group from Buca della Vena mine, Tuscany, Italy. *Am. Mineral.*, **82**, 807–811.

Orlandi, P., Pasero, M., Rotiroti, N., Olmi, F., Demartin, F., Moëlo, Y. (2004): Gramacciolite-(Y), a new mineral of the crichtonite group from Stura Valley, Piedmont, Italy. *Eur. J. Mineral.*, **16**, 171–175.

Oxford Diffraction (2002): CrysAlis CCD and CrysAlis RED. Versions 1.69. Oxford Diffraction, Oxford, England.

Peun, T., Zinn, P., Lauterjung, J., Hinze, E. (1995): In-situ X-ray diffraction experiments with MAX-80 using synchrotron radiation. *Bochumer geol. geotechn. Arb.*, **44**, 139–144.

Pouchou, L. J. & Pichoir, F. (1984): New model quantitative x-ray microanalysis, 1. Application to the analysis of homogeneous samples. *Rech. Aerosp.*, **3**, 13–38.

Ring, U. & Layer, P.W. (2003): High-pressure metamorphism in the Aegean, eastern Mediterranean: Underplating and exhumation from the Late Cretaceous until the Miocene to Recent above the retreating Hellenic subduction zone. *Tectonics*, **22**, 1022–1045.

Schmitt, R.A., Smith, R.H., Olehy, D.A. (1964): Rare-earth, yttrium and scandium abundances in meteoritic and terrestrial matter – II. *Geochim. Cosmochim Acta*, **28**, 67–86.

Shannon, R.D. (1976): Revised effective ionic radii and systematic studies of interatomic distances in halides and chalcogenides. *Acta Cryst.*, **A32**, 751–767.

Sheldrick, G.M. (1997): SHELXTL-97. Univ. Göttingen, Germany.

Wang, L., Essene, E.J., Zhang, Y. (1999): Mineral inclusions in pyrope from Garnet Ridge, Arizona, USA: implication for processes in the upper mantle. *Contrib. Mineral. Petrol.*, **135**, 164–178.

Wang, X. & Liebau, F. (1996): Studies on bond and atomic valences. I. Correlation between bond valence and bond angles in Sb^{III} chalcogen compounds: the influence of lone-electron pairs. *Acta Cryst.*, **B52**, 7–15.

Will, T., Okrusch, M., Schmädicke, E., Chen, G. (1998): Phase relations in the greenschist-blueschist-amphibolite-eclogite facies in the system $Na_2O-CaO-FeO-MgO-Al_2O_3-SiO_2-H_2O$ (NCFMASH), with application to metamorphic rocks from Samos, Greece. *Contrib. Mineral. Petrol.*, **132**, 85–102.

Wilson, A.J.C. (1992): International Tables for X-ray Crystallography, Vol. C, Kluwer Academic Press, London, 883 p.

Wülser, P.-A., Meisser, N., Brugger, J., Schenk, K., Ansermet, S., Bonin, M., Bussy, F. (2005): Cleusonite, $(Pb,Sr)(U^{4+},U^{6+})(Fe^{2+},Zn)_2(Ti,Fe^{2+},Fe^{3+})_{18}(O,OH)_{38}$, a new mineral species of the crichtonite group from the western Swiss Alps. *Eur. J. Mineral.*, **17**, 933–942.

Received 29 May 2009

Modified version received 6 November 2009

Accepted 29 January 2010